Coherence time of over a second in a telecom-compatible quantum memory storage material

Miloš Rančić,[1,*] Morgan P. Hedges,[2] Rose L. Ahlefeldt,[1] and Matthew J. Sellars[1]

[1] *Centre for Quantum Computation and Communication Technology, Laser Physics Centre, The Australian National University, Canberra, Australian Capital Territory 0200, Australia*

[2] *Physics, Princeton University, Princeton, New Jersey 08554, USA.*

arXiv:1611.04315v1 [quant-ph] 14 Nov 2016

Quantum memories for light will be essential elements in future long-range quantum communication networks. These memories operate by reversibly mapping the quantum state of light onto the quantum transitions of a material system. For practical applications it is necessary for the quantum coherence times of these transition to be long compared to the network transmission times. For a global communication network this will be of the order of 100 ms. Due to a lack of a suitable storage material, a quantum memory that operates in the 1550 nm optical fiber communication band with a storage time greater than 50 ns has yet to be demonstrated.

Here we describe the spin dynamics of $^{167}Er^{3+}:Y_2SiO_5$ in a high magnetic field and demonstrate that this material has the necessary characteristics for a practical quantum memory operating in the 1550 nm communication band. We observe a hyperfine coherence time of 1.3 seconds. Further, we demonstrate efficient optical pumping of the entire ensemble into a single hyperfine state, the first such demonstration in a rare-earth system and a requirement for broadband spin-wave storage. With an absorption of 70 dB/cm at 1538 nm and Λ transitions enabling spin-wave storage, this material is the first candidate identified for an efficient, broadband quantum memory at telecommunication wavelengths.

Any future globally deployed quantum communication network [1, 2] will require nodes connected by optical fiber. To minimise transmission loss and maintain high data throughput, all elements of such a network, particularly quantum repeater nodes, should operate in one of the low loss telecom bands for optical fiber at 1310 and 1550 nm. In its simplest implementation, a quantum repeater relies on an efficient, long-lived quantum memory [3]. Developing such a memory is, in itself, very challenging and to date no proposed implementation has been able to satisfy the additional requirement of compatibility with the low loss telecom bands.

The potential for developing practical quantum memories based on rare-earth ions has been highlighted through a series of recent demonstrations using non-Kramers ions (ions with an even number of electrons). Crystals doped with either praseodymium or europium have demonstrated spin-wave storage of quantum states of light [4], multimode storage [5], large efficiencies [6, 7] and hyperfine coherence times of 6 hours using the Zero First Order Zeeman (ZEFOZ) technique [8]. The success of these demonstrations relies on the fact that the electronic angular momenta of non-Kramers ions can be quenched by the crystal field for sites with sufficiently low symmetry. As a consequence, these ions can exhibit the long ground-state hyperfine lifetimes necessary for efficient optical spin pumping and long hyperfine coherence times. These properties are key to the successful operation of efficient, long lived quantum memories. Unfortunately for communication applications, none of the non-Kramers ions have suitable optical transitions in any of the fiber telecom bands.

Erbium does have an optical transition at 1538 nm, but is a Kramers ion (odd number of electrons). To date, there has been no demonstration of an on-demand quantum memory in a Kramers system. The root of the difficulty is that, unlike for non-Kramers, the electronic magnetic moment of Kramers ions cannot be quenched by a crystal field as they possess a half-integer spin. For these ions there is a rapid electronic spin relaxation which shortens the hyperfine state lifetimes. Baldit et al. found the hyperfine state lifetimes to be limited to 100 ms when demonstrating electromagnetic induced transparency in $^{167}Er^{3+}$:Y_2SiO_5 [9]. This is similar to the electron spin lifetime [10] and only an order of magnitude longer than the optical excited state lifetime, making efficient optical spin pumping impossible. In comparison, the hyperfine lifetimes for Pr^{3+}:Y_2SiO_5 and Eu^{3+}:Y_2SiO_5 are 5 minutes and 23 days respectively [11, 12].

Nevertheless, there has been considerable work towards developing quantum memories using erbium. The general strategy has been to avoid spin-wave storage of the quantum states and instead store only on the optical transition. Atomic Frequency Comb (AFC) delay lines have delayed quantum states of light in Er doped glass fiber [13], however, the efficiency was limited to ~ 1 % and the storage time to 50 ns. Weak coherent states have also been stored in crystals using a two-level Gradient Echo Memory (GEM) technique with an efficiency of 0.25%. The fidelity of the recalled state in this demonstration was, however, below the non-classical limit [14]. For both these demonstrations the

* Corresponding author (milos.rancic@anu.edu.au)

inefficiency of the optical pumping of the ground state electron spin levels were identified as limiting the memories' efficiency. To avoid this limitation, new on-demand memory techniques not requiring optical pumping to initialize the ensemble have been proposed and demonstrated [15, 16]. Although these techniques have shown significantly higher efficiencies, up to 40%, the storage times are still limited by the optical coherence time and quantum storage has yet to be demonstrated. Currently, there is no proposed strategy to achieve the fidelities and storage times required for quantum repeater applications [17] without using long lived hyperfine states.

Here, we investigate the hyperfine spin dynamics of $^{167}Er^{3+}$:Y_2SiO_5 in the presence of a large magnetic field, with the aim of increasing both the hyperfine lifetime and coherence time to be comparable to non-Kramers systems. As mentioned above, the hyperfine lifetime is short because it is coupled to the electron spin, which itself flips rapidly due to coupling to the lattice and to other electron spins. In order to increase the hyperfine lifetime, therefore, it is necessary to slow the electron spin flips. Böttger et al. previously demonstrated that applying a sufficiently large magnetic field can suppress electron spin flips in Er^{3+}:Y_2SiO_5 [18]. The field decreases both the spin-lattice contribution and the spin-spin contribution. The spin-lattice is turned off because, with the electron spin splitting much larger than kT, the energy density of available phonons is low (see Figure 4). In other words, the electron spin is frozen into the lower spin state. This also turns off the spin-spin interaction, since there are no ions in the upper spin state to allow a spin flip-flop. Although the spin is frozen, the lifetime of the excited electron spin state is, in fact, shorter than at low field because of the large density of empty phonon modes available for an excited spin to decay into. This short lifetime has limited the usefulness of this technique for previous memory demonstrations. However, these demonstrations worked with the $I = 0$ Er isotopes, and here we show that the situation is very different for ^{167}Er with $I = 7/2$. Once the electron spin is frozen in the lower ground state, the hyperfine levels associated with this state can have extremely long lifetimes and coherence times.

The material used for this investigation is a 0.005% doped $^{167}Er^{3+}$:Y_2SiO_5 crystal, enriched to 92% isotopic purity. To most easily access the regime where the electron spin is frozen, the crystal was oriented with the magnetic field along the D_1 optical extinction axis. This direction was chosen because the anisotropic g-factor of Er^{3+}:Y_2SiO_5 is almost maximum along this axis, with a ground-state splitting of 214 GHz/T [19]. The ground state hyperfine structure was studied optically by exciting the $^4I_{15/2} \rightarrow {}^4I_{13/2}$ optical transition between the two spin-down projections of the lowest crystal field level, at wavelength of 1538 nm. In a field of 7 T, the Zeeman splitting of the electronic spin projections is more than sufficient to resolve this transition. With a nuclear moment of $I = 7/2$, ^{167}Er exhibits eight hyperfine spin states $m_I = |-7/2\rangle, \cdots, |+7/2\rangle$

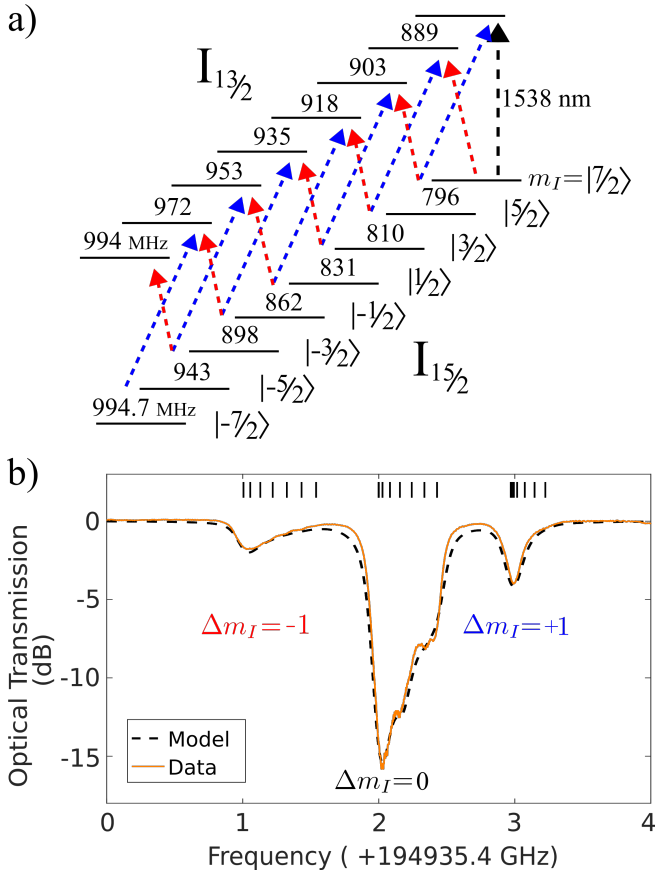

Figure 1. a) 1538 nm optical transition level diagram for $^{167}Er^{3+}$: Y_2SiO_5 in a field of 7 T. The red-detuned $\Delta m_I = -1$ transitions are represented by red arrows, and blue arrows for $\Delta m_I = +1$. The energy spacing between the hyperfine states was determined by holeburning. b) ***Orange:*** Absorption spectrum at 1.4 K with a field of 7 T along the D_1 axis. ***Black:*** model of absorption based on holeburning measurements. ***Vertical Black Dashes:*** The centroids of the optical transitions used in the black spectrum model.

and the entire system studied comprises sixteen energy levels, as shown Figure 1 a). The hyperfine energy spacings were obtained by hole-burning measurements.

The absorption spectrum of the optical transition is shown in Figure 1 b). Three bands are clearly resolved in this spectrum, which we associate with the $\Delta m_I = -1, 0$ and 1 transitions. A model of the Er^{3+} population was developed based on the energy splittings and absorption spectrum in Figure 1. In this model, the inhomogeneous broadening of the population was described by a Voigt profile that was fitted with equal Gaussian and Lorentzian contributions, and a linewidth of 150 MHz. The contribution of the Er^{3+} impurity isotopes is included, with a transition energy near the centre of the $\Delta m_I = 0$ hyperfine transitions. The absorption distribution derived from the population model is shown by the black trace in Figure 1 b). The oscillator strengths for each hyperfine transition were

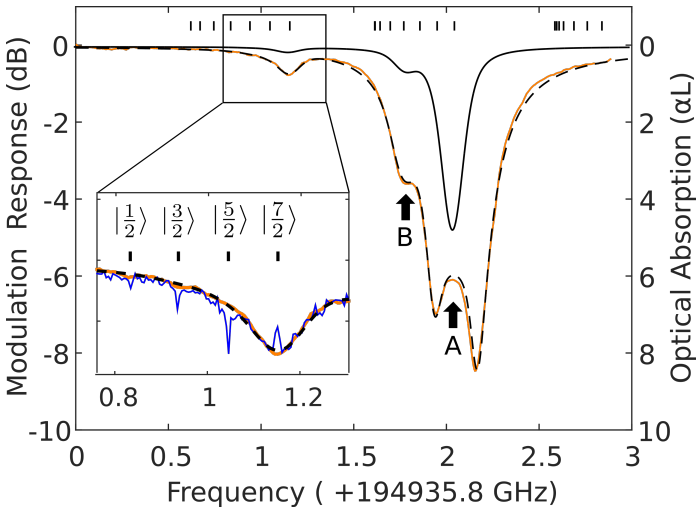

Figure 2. Absorption spectrum of $^{167}Er^{3+} : Y_2SiO_5$ with 95% of the ensemble pumped into the $|+7/2\rangle$ hyperfine spin state ***(Orange***), obtained by AM spectroscopy. Pumping into the $m_I = |+7/2\rangle$ state was achieved by sweeping an EOM sideband over the set of $\Delta m_I = +1$ transitions, corresponding to 2.4 - 3.0 GHz frequency region. Arrow **A** indicates the centre of the $|+7/2\rangle \rightarrow |+7/2\rangle$ absorption line. Arrow **B** indicated absorption of isotopic impurities. ***Black Solid Trace:*** Theoretical model of optical absorption. ***Black Dashed Trace:*** Theoretical model of the Radio Frequency (RF) modulation response. ***Black Vertical Dashes:*** Centroids of inhomogeneously broadened optical transitions, upon which the model is based. ***Inset (Orange):*** An expanded view of the $\Delta m_I = -1$ transitions. ***Inset (Dark Blue):*** Upon holeburning at the peak absorption shown by arrow **A**, a hole and a series of anti-holes are generated at the predicted energies. The labeled dashes indicate the hyperfine ground state for each transition.

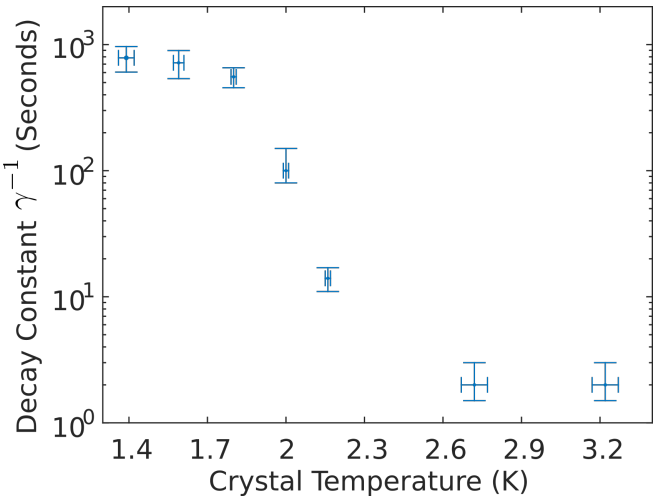

Figure 3. Decay of spin polarisation as a function of temperature, in a field of 7 T. The value of γ^{-1} is the hyperfine population decay rate (T_1).

determined from the fit to the spectrum in orange, assuming equal population in each hyperfine spin level. Whilst the strongest optical transitions are those that conserve the nuclear magnetic moment ($\Delta m_I = 0$), there is appreciable oscillator strength in the fourteen $\Delta m_I = \pm 1$ transitions. Relative to the $\Delta m_I = 0$ transitions, the oscillator strengths for $\Delta m_I = -1\,(+1)$ start at approximately 25% (33%) for transitions involving the $|-7/2\rangle$ states, and decrease linearly to about 2.5% (3.3%) for the $|+7/2\rangle$ states. The decrease can be attributed to a difference in mixing between hyperfine levels across the series.

With the $\Delta m_I = -1$ and $+1$ bands clearly resolved, pumping of the nuclear spin into a single state is possible through frequency selection. By exciting only the seven $\Delta m_I = +1$ transitions (the peak at 3 GHz in Figure 1 a), we were able to pump $95 \pm 3\%$ of the ^{167}Er population into the $|+7/2\rangle$ hyperfine ground state. This results in a nearly eight-fold increase in the already high optical depth of this transition. Such a high optical depth is difficult to measure accurately with traditional absorption spectroscopy, and instead Amplitude Modulation (AM) spectroscopy was used. This method is sensitive to both the absorption and the phase shift of the transmitted light, allowing a more accurate determination of the optical depth (for more detail, refer to the Materials and Methods section).

The resulting spectrum is shown in Figure 2. Also shown in this figure is the model fitted to the spectrum to obtain the optical depth, and the resulting absorption lineshape. This absorption line has two components – a shoulder at arrow B due to the impurity isotopes, and a central peak at A due to ions in the $m_I = |+7/2\rangle$ state. The AM spectrum for this peak has a central dip due to the changing phase of the transmitted light as the laser was swept through the highly absorbing peak. At this frequency the absorption was determined to be 70 ± 4 dB/cm

When hole-burning at the frequency of arrow A, the blue spectrum in the inset of Figure 2 is observed. The hole and anti-holes demonstrate that spin-pumped population is shifted into $|+5/2\rangle, |+3/2\rangle$ and $|+1/2\rangle$ hyperfine levels via the $\Delta m_I = -(1, 2\,\&\,3)$ optical decay paths.

The efficiency of the spin-pumping ($95 \pm 3\%$) was measured by the fitting the model to only the $\Delta m_I = -1$ transitions, where the decreasing trend in oscillator strengths and low absorption improve the accuracy of the population estimate. The ability to polarise the ^{167}Er ensemble into a single hyperfine state opens the path towards several high-bandwidth memory techniques, which are discussed later.

Once the ^{167}Er ensemble is pumped into the $|+7/2\rangle$ hyperfine state, the population slowly relaxes to thermal equilibrium. Two processes were identified as contributing to the relaxation, both of which are phonon-mediated. The first is direct hyperfine-phonon coupling involving GHz phonons and the second is the THz electronic-phonon process discussed previously [20].

To first order, these processes only cause decay through the $\Delta m_I = \pm 1$ hyperfine transitions. This allowed us to model the population dynamics as a series of coupled rate

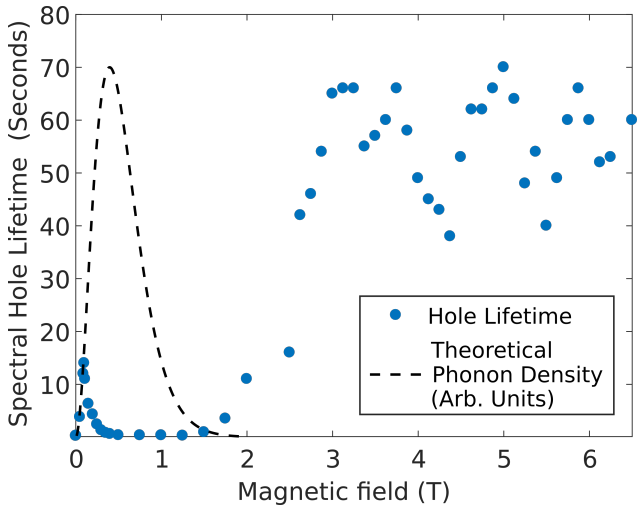

Figure 4. Spectral hole lifetime at 1.4 K, as a function of magnetic field along the D_1 axis. The theoretical phonon density in black is a thermal Planck distribution. The curve assumes the Zeeman splitting determined by T. Böttger [19].

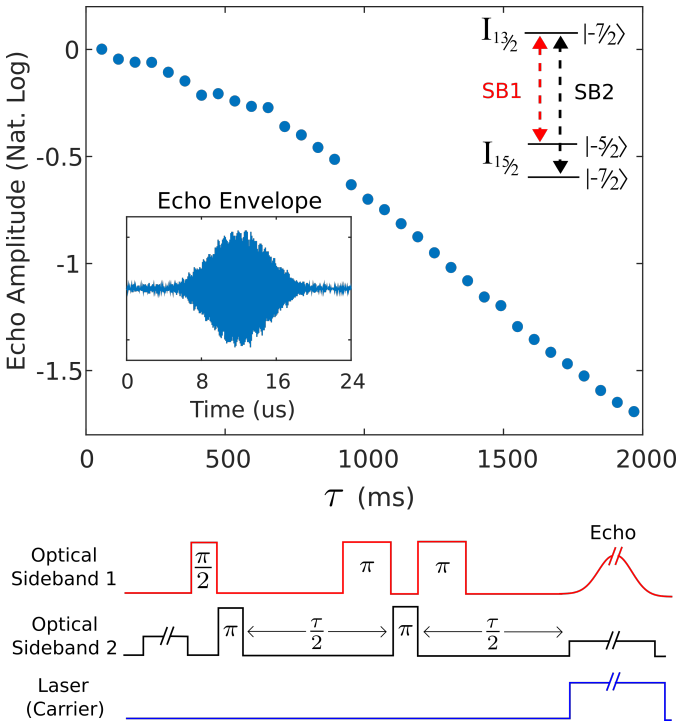

Figure 5. Normalised Raman echo intensity as a function of total delay τ, at 1.4 K and 7 T. For the Raman Echo sequence, the laser sits approximately 1 GHz detuned from the lowest energy transitions, to prevent any absorption. The two optical fields required to drive the ions were provided by the sidebands of the same EOM used for AM spectroscopy, at 1155.3 MHz (SB1) and 2150 MHz (SB2). The carrier acted as a local oscillator to optically detect the Raman echo. (Refer to Materials and Methods for the more detail). ***Inset:*** The Raman echo time envelope with $\tau = 60$ ms.

equations, with the same coupling rate γ between all adjacent hyperfine states. This population-dynamics model accurately fit the recorded time series of spectra, hence supporting the assumptions of the dynamics.

The result of this fitting is shown Figure 3, where a time series was recorded at each temperature plotted. The figure shows an exponential increase in T_1 from 2.2 $\rightarrow$ 1.8 K. This agrees with the exponential reduction in high energy phonons from the Planck distribution and therefore indicates that the Raman phonon process dominates in this temperature region. The plateau in transition lifetimes below 1.8 K is attributed to direct hyperfine-phonon coupling, which is independent of temperature in this regime. Above 2.6 K, the plateau in lifetimes is consistent with the presence of a phonon bottleneck, limiting the rate of hyperfine relaxation [20].

The other important decay mechanism in this system is hyperfine spin-spin cross-relaxation. This process is masked in the previous measurement because it does not redistribute the hyperfine populations, and therefore does not change the population envelope. However, it will affect any measurements operating on a sub-group of the entire ensemble, in particular spectral holeburning. Since spectral shaping via holeburning is a vital component of many quantum memory applications, it is important to characterise the cross relaxation process.

We studied hyperfine cross-relaxation by measuring the lifetime of a spectral hole burnt in the unpolarised spin ensemble as a function of magnetic field. As shown in Figure 4, the hole lifetime is short for fields below 3 T. In this regime, the electron spin is not yet frozen and electron spin effects dominate the hole lifetime. There is a small peak in the lifetime at 0.1 T, corresponding to the field where the electronic Zeeman splitting is large enough that electron spin cross relaxation has been slowed, but where the phonon energy density is still low. As the phonon density increases, the lifetime drops, increasing only as the density drops back down near zero at around 3 T. Above 3 T, hyperfine cross-relaxation dominates the hole lifetime, leading to a maximum lifetime of about 70 s. The hole lifetime does vary with field above 3 T, which is not expected in a simple model of resonant hyperfine cross-relaxation. We attribute the variation to the existence of fields where the detuning between different Er hyperfine transitions can be bridged by an Y ion spin flip, increasing the pool of ions a given ion can cross-relax with.

We have shown that applying a large magnetic field freezes out the electron spin dynamics. This results in a much quieter magnetic environment in the crystal. Since magnetic field fluctuations typically dominate the hyperfine coherence time, this should lead to a substantial increase in the coherence time from its zero field value of 1 μs [9].

We investigated the coherence time on the $|-7/2\rangle \leftrightarrow |-5/2\rangle$ ground state transition at 7 T using an all-optical Raman echo technique. With this pulse sequence, coherence be-

tween hyperfine states is established and manipulated via a common optical excited state, rather than by direct magnetic resonance. One advantage of this technique is that the bandwidth of the $\sim 1\,\mu s$ optical pulses used is much larger than the inhomogeneous broadening of the hyperfine transition, and so the width of the echo envelope gives a direct measure of this inhomogeneous broadening. As shown in the inset to Figure 5, the echoes had a FWHM of $7\pm1\ \mu$s, corresponding to an inhomogeneous linewidth of 800 ± 100 kHz.

The decay of the echo amplitude with time is also shown in Figure 5. Below 1 second, the decay is sub-exponential. Given this, we define the coherence time as the time at which the echo amplitude has decayed to e^{-1} of its original value, giving $T^*_{2\,(echo)} = 1300 \pm 10$ ms.

With the electron spin frozen, this coherence time will be dominated by the dynamics of the nuclear spins in the crystal, principally the Y ions. Following the approach of Zhong et al. [8], we can estimate the coherence time expected at this field given the Zeeman coefficient, which we measured to be 5.6 MHz/T along this D_1 direction. Assuming a rapid Y spin relaxation rate, the induced magnetic broadening should limit the coherence time to 70 ms, much shorter than we observe. The discrepancy indicates that a large number of the Y spins are flipping much slower than the bulk rate. This is due to the presence of a large frozen core of Y spins around the Er site that have been detuned from the bulk by the large magnetic field from the Er ion. Further evidence for the frozen core is provided by the non-exponential decay of the echo, which can be attributed to spectral diffusion caused by the slow Y spin flips within the frozen core.

Here, we have shown that applying a large magnetic field of 7 T can extend the hyperfine coherence time of Er to 1.3 seconds. In fact, Figure 4 indicates that a similar result could be achieved at fields as low as 3 T. This value is comparable to the longest coherence times obtained in non-Kramers systems using the well known ZEFOZ technique [8]. From a practical standpoint, the technique shown here has an advantage over ZEFOZ, since it does not require precise alignment of the magnetic field.

In the context of quantum repeater applications, the coherence time seen here has surpassed an important limit. Ravazi et al. show that a coherence time of 1 second is more than sufficient for a 1000 km quantum repeater network, even without error correction [17]. From their analysis we determine it sufficient, in fact, to establishing a global repeater network (a distance of 10,000 km).

This system could also be considered for applications requiring long term storage, i.e: a quantum 'hard-drive'. For this application, it should be possible to achieve a coherence time approaching the population T_1 limit (10 minutes) at 1.6 K and 7 T using ZEFOZ. At first glance it might seem the coherence time should be limited to approximately one minute given the hyperfine cross-relaxation rate of 70 s we measured here. However, cross-relaxation predominantly couples adjacent hyperfine levels ($\Delta m_I = \pm 1$); it is highly suppressed for transitions with $|\Delta m_I| > 1$. One can take advantage of this by preparing storage qubits using non-adjacent hyperfine levels, for instance $|-7/2\rangle \leftrightarrow |-3/2\rangle$. By intialising (pumping) the ensemble into a single hyperfine level and 'shelving' flying qubits (optical excitation) onto a non-adjacent level, a Λ system is formed with a storage lifetime no longer limited by hyperfine cross-relaxation.

Finally, the ability to efficiently pump the ^{167}Er ensemble into a single hyperfine state is crucial for high-bandwidth quantum communication. It paves the way for broadband Raman memory techniques which, until now, have been limited to atomic vapour systems [21] and potentially nitrogen vacancies in diamond [22]. Alternatively, spin-pumping allows for potentially GHz-bandwidth spin-wave storage using techniques already demonstrated in rare earth systems, such as GEM [6] and drastically improves the efficiency of AFC delay lines [23].

Materials and Methods:

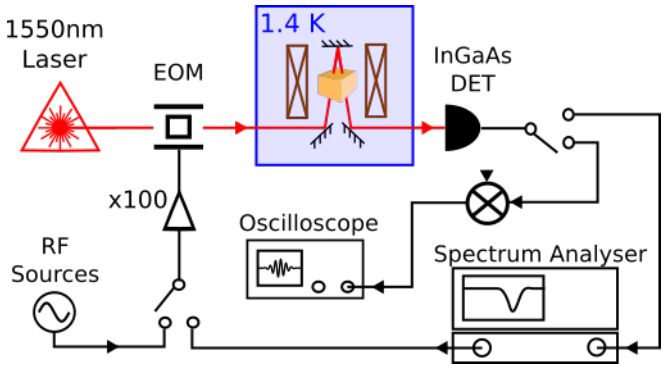

Figure 6. The combined experimental setup for all measurements recorded. In all cases, the light source used was a single frequency stabilised laser and two optical sidebands generated by either an amplitude or phase modulating EOM. A series of TTL RF switches were used to alternate between RF sources (and measurement devices). Three tunable single-frequency RF sources were available to generate short optical pulses as well as a VCO for hyperfine spin-pumping. Most spectra were recorded on the spectrum analyser using AM spectroscopy. Echo measurements were recorded on the oscilloscope by mixing GHz optical modulation and RF to generate a 10 MHz signal.

Experimental Setup

As shown in Figure 6, a 0.005% doped $^{167}Er^{3+}$:Y_2SiO_5 $3 \times 4 \times 5$ mm (D_1,D_2,b) crystal provided by Scientific Materials Corp (Bozeman, Montana) was maintained at 1.4 K in an Oxford helium bath cryostat with a 15 T superconducting magnet. Both the magnetic field and light propagating direction were parallel with the D_1 optical extinction axis. As there was only one cryostat window, the crystal was placed against a mirror, onto which the beam was focused with a 70 μm waist. The reflection down the D_1 axis gave a total absorption length of 6mm. The op-

tical transition were excited with a Thorlabs TLK-1550R laser, stabilised to a home-made fiber reference cavity with a 1 second linewidth less than 100 kHz. Intensity and frequency modulation of the light was achieved with a 10 GHz JDSU AM-EOM and detected with a Lab Buddy 10 GHz detector.

AM Spectroscopy

This method was based on detecting the optical beat between the sidebands and carrier of an EOM as a function of the modulation frequency. The RF modulation sweep was generated by a spectrum analyser, which was also used for detection. This formed a closed modulation loop, as shown in Figure 6. The optical sidebands are weak ($\sim 1\%$) compared to the carrier power and the laser is kept far detuned ($0.5 - 1$ GHz) from the absorption.

This technique is phase sensitive, allowing for accurate measurement of large optical depths, and as the laser remains locked to the reference cavity spectra can be recorded in conjunction with precise optical pulses and sweeps.

Energy Structure and Spin Pumping

The hyperfine structure of the $I_{15/2}$ and $I_{13/2}$ states were determined at 7 T and 1.4 K through a series of holeburning measurements. A 0 to 4 GHz tunable RF source was used to generated a series of 20 spectral holes across 3 sets of measurements. Each spectrum was made by applying fixed-frequency RF for 100 ms. The absorption spectrum was recorded by a 0.01 to 2.9 GHz RF scan with the tracking generator and RF input on the spectrum analyser (50 ms scan, 1 MHz RBW).

To spin pump the ensemble into either the $m_I = |{}^{+7}/_{2}\rangle$ or $|{}^{-7}/_{2}\rangle$ hyperfine ground state, a Voltage Controlled Oscillator (VCO) was used to drive the EOM. A 3 second saw-tooth scan (100 ms rep rate) was performed over the $\Delta m_I = -1$ or $+1$ absorption bands respectively, with $\sim$2 mW of optical power in each sideband. The spin-pumped absorption spectrum was recorded once again using AM spectroscopy. Repeating this with the laser (carrier) frequency on either side of the absorption feature, it was possible to stitch two scans together to span more than 2.9 GHz, as shown in the light blue trace of Figure 2.

Magnetic Field Dependence of Spectral Holes

Spectral holes were burnt into the centre of the $\Delta m_I = +1$ absorption band, as it afforded better optical depth than the $\Delta m_I = -1$ band and better holeburning characteristics than the $\Delta m_I = 0$ band. Between 0 and 1.5 T, spectral holes were generated using a tunable RF source and measured using AM spectroscopy. Above 1.5 T, 5 MHz wide spectral trenches were burnt instead, as there was negligible spectral diffusion and long hole-burning lifetimes. This was achieved by sweeping the spectrum analyser tracking generator output over 5 MHz for 10 seconds. The tracking generator output was centred at approximately 1.5 GHz to keep the laser carrier and second sideband off-resonant.

Temperature Dependence of Spin Pumping

In a 7 T field, spin pumping into the $m_I = |{}^{+7}/_{2}\rangle$ state was achieved using the same technique as described above. At each temperature, 5 to 6 spectra were recorded at time intervals spaced long enough to observe appreciable relaxation back to thermal equilibrium. For example, at 1.6 K, spectra were recorded after 10 seconds and (10, 20, 40, 80) minutes.

Optical Raman Echoes

Optical pulses (π & $\pi/2$) were generated using the EOM sidebands and two RF generators tuned to 1155.3 MHz and 2150 MHz. The pulse lengths were optimised using two pulse optical echoes at either frequency, with 1.5 mW of optical power in each sideband. For the $|I_{15/2}, {}^{-5}/_{2}\rangle \leftrightarrow |I_{13/2}, {}^{-7}/_{2}\rangle$ transition (1155.3 MHz), the optimal π-pulse length is $4 \pm 0.5\,\mu$s and for the $|I_{15/2}, {}^{-7}/_{2}\rangle \leftrightarrow |I_{13/2}, {}^{-7}/_{2}\rangle$ a π-pulse was 1.5 μs (2150 MHz). The hyperfine spin ensemble was prepared by first pumping into the $m_I = |{}^{-7}/_{2}\rangle$ state with a VCO for 10 seconds, as described above. This was followed by applying a 100 μW pulse at 2150 MHz for 100 ms, to generate a 100 kHz wide absorption feature (anti-hole) in the $m_I = |{}^{-5}/_{2}\rangle$ subgroup. After the pulse sequence, the echo that reformed at the wavelength of the 1150 MHz sideband was detected as a 1155.3 MHz optical beat between the sideband and the carrier. This RF signal was then mixed with a 1145.3 MHz RF source, and the 10 MHz beat signal was recorded on a Tektronix 500 MHz oscilloscope. Note: The detected echo amplitude in this technique depends on the proportion of the initial ensemble transferred into the optical $|-{}^{7}/_{2}\rangle \leftrightarrow |-{}^{7}/_{2}\rangle$ transition, which is determined by the probing power of sideband 2.

Acknowledgements

M. J. S would like to acknowledge C. Thiel for insightful discussions. This work was supported by the Australian Research Council Centre of Excellence for Quantum Computation and Communication Technology (Grant No. CE110001027). M. J. S. was supported by an Australian Research Council Future Fellowship (Grant No. FT110100919).

Author Contributions

M. J. S and M. P. H. conceived the initial project. M. J. S, M. P. H and M. R. designed the experimental setup. M. R. carried out the experiment. M. R and R. L. A. analysed the results. The manuscript was written by M. J. S and M. R. and R. L. A.

[1] N. Gisin and R. Thew, Nature Photonics **1**, 165 (2007).

[2] H. J. Kimble, Nature **453**, 1023 (2008).

[3] L. M. Duan, M. D. Lukin, J. I. Cirac, and P. Zoller, Nature **414**, 413 (2001).

[4] K. R. Ferguson, S. E. Beavan, J. J. Longdell, and M. J. Sellars, Physical Review Letters **117**, 020501 (2016).

[5] C. Laplane, P. Jobez, J. Etesse, N. Timoney, N. Gisin, and M. Afzelius, New Journal of Physics **18**, 013006 (2015).

[6] M. P. Hedges, J. J. Longdell, Y. Li, and M. J. Sellars, Nature **465**, 1052 (2010).

[7] M. Sabooni, Q. Li, S. Kröll, and L. Rippe, Physical Review Letters **110**, 133604 (2013).

[8] M. Zhong, M. P. Hedges, R. L. Ahlefeldt, J. G. Bartholomew, S. E. Beavan, S. M. Wittig, J. J. Longdell, and M. J. Sellars, Nature **517**, 177 (2015).

[9] E. Baldit, K. Bencheikh, P. Monnier, S. Briaudeau, J. A. Levenson, V. Crozatier, I. Lorgeré, F. Bretenaker, J. L. Le Gouët, O. Guillot-Noël, and P. Goldner, Physical Review B **81**, 144303 (2010).

[10] S. R. Hastings-Simon, B. Lauritzen, M. U. Staudt, J. L. M. van Mechelen, C. Simon, H. de Riedmatten, M. Afzelius, and N. Gisin, Physical Review B **78**, 085410 (2008).

[11] K. Holliday, M. Croci, E. Vauthey, and U. P. Wild, Physical Review B **47**, 14741 (1993).

[12] F. Könz, Y. Sun, C. W. Thiel, R. L. Cone, R. W. Equall, R. L. Hutcheson, and R. M. Macfarlane, Physical Review B **68**, 085109 (2003).

[13] E. Saglamyurek, J. Jin, V. B. Verma, M. D. Shaw, F. Marsili, S. W. Nam, D. Oblak, and W. Tittel, Nature Photonics **9**, 83 (2015).

[14] B. Lauritzen, J. Minár, H. de Riedmatten, M. Afzelius, N. Sangouard, C. Simon, and N. Gisin, Physical Review Letters **104**, 080502 (2010).

[15] J. Dajczgewand, J.-L. Le Gouët, A. Louchet-Chauvet, and T. Chanelière, Optics Letters **39**, 2711 (2014).

[16] G. Hétet, J. J. Longdell, A. L. Alexander, P. K. Lam, and M. J. Sellars, Physical Review Letters **100**, 023601 (2008).

[17] M. Razavi, M. Piani, and N. Lütkenhaus, Physical Review A **80**, 032301 (2009).

[18] T. Böttger, C. W. Thiel, R. L. Cone, and Y. Sun, Physical Review B **79**, 115104 (2009).

[19] T. Böttger, *Laser frequency stabilization to spectral hole burning frequency references in erbium-doped crystals : material and device optimization*, Ph.D. thesis, Montana State University (2002).

[20] A. Abragam and B. Bleaney, *Electron Paramagnetic Resonance of Transition Metal Ions*, 2nd ed. (Dover Publications, 1970) pp. 541–550, 574–583.

[21] D. J. Saunders, J. H. D. Munns, T. F. M. Champion, C. Qiu, K. T. Kaczmarek, E. Poem, P. M. Ledingham, I. A. Walmsley, and J. Nunn, Physical Review Letters **116**, 090501 (2016).

[22] E. Poem, C. Weinzetl, J. Klatzow, K. T. Kaczmarek, J. H. D. Munns, T. F. M. Champion, D. J. Saunders, J. Nunn, and I. A. Walmsley, Physical Review B **91**, 205108 (2015).

[23] H. de Riedmatten, M. Afzelius, M. U. Staudt, C. Simon, and N. Gisin, Nature **456**, 773 (2008).